Inorg. Chem. **2007**, *46*, 10659–10669

Inorganic Chemistry

Article

Electron Transfer Activity of Nickelacyclic Complex Analogues of Nickelocene: Synthesis of (η^5-R-cyclopentadienyl){η^4-[1-(η^5-R-cyclopentadienyl)]-2,3,4,5-tetraphenyl-1-nickela-2-cyclopentenyl}nickel Complexes (R = H, CH_3) and Crystal Structures of the Redox Couples [(η^5- Methylcyclopentadienyl){η^4-[1-(η^5-methylcyclopentadienyl)]-2,3,4,5-tetraphenyl-1-nickela-2-cyclopentenyl}nickel]$^{(0/+)}$ and [(η^5-Methylcyclopentadienyl){η^5-[1-(η^5-methylcyclopentadienyl)-1-nickelafluorenyl}nickel]$^{(0/+)}$

Serena Losi,[†] Fulvio Rossi,[†] Franco Laschi,[†] Fabrizia Fabrizi de Biani,[†] Piero Zanello,*[,†] Piotr Buchalski,*[,‡] Kinga Burakowska,[‡] Katarzyna Piwowar,[‡] Jolanta Zbrzezna,[‡] Stanisaw Pasynkiewicz,[‡] Antoni Pietrzykowski,[‡] Kinga Suwińska,[§] and Lucjan Jerzykiewicz[||]

Dipartimento di Chimica, Università di Siena, Via De Gasperi 2, 53100 Siena, Italy, Warsaw University of Technology, Faculty of Chemistry, Koszykowa 75, 00-662 Warsaw, Poland, Institute of Physical Chemistry of the Polish Academy of Sciences, Kasprzaka 44/52, 01-224 Warsaw, Poland, and Faculty of Chemistry, University of Wrocaw, Joliot-Curie 14, 50-353 Wrocaw, Poland

Received June 22, 2007

Following previous reports on the synthesis and structure of different nickelacyclic complexes analogues of nickelocene, we now deal with the new metallacyclic compounds (η^5-R-cyclopentadienyl){η^4-[1-(η^5-R-cyclopentadienyl)]-2,3,4,5-tetraphenyl-1-nickela-2-cyclopentenyl}nickel (R = H, CH_3). The redox ability of the whole series of nickelacyclic derivatives has been also investigated by electrochemical and spectroelectrochemical techniques, and the nature of the frontier orbitals responsible for the rich electron transfer activity of this class of compounds has been supported by theoretical considerations. On the basis of the redox properties of a few neutral members of the series, their chemical oxidation afforded the corresponding monocations and the crystal structures of the pertinent redox couples were determined by X-ray single-crystal analysis.

Introduction

Nickelocene, which is the metallocene possessing the highest number of valence electrons (i.e., 20), is an excellent starting material for the synthesis of cyclopentadienylnickel complexes useful in catalysis.[1,2,3] It is quite reasonable to expect that nickelocene analogues such as metallametallocenes, in which one cyclopentadienyl group of metallocene is replaced by a metallacyclopentadienyl ring,[4] may also display interesting features.

Some of us have already reported on the indenyl and fluorenyl nickelanickelocenes **1**,[5] **2**,[6] and **3** and **4**,[7] Chart 1, in which the metalated rings are bonded to the central nickel atom in η^3 or η^5 manner.

In this paper we present the characterization of the new complexes **5a**,**b**, Chart 2, in which the central nickel atom is sandwiched between a cyclopentadienyl and a nickelacyclopentenyl ring.

On the basis of the electrochemical and spectroelectrochemical behavior of complexes **2**−**5**, compounds **4** and **5b** were chemically oxidized (by $[Cp_2Fe]^+PF_6^-$) to their monocations $\mathbf{4^+PF_6^-}$ and $\mathbf{5b^+PF_6^-}$, respectively, and the X-ray crystal structures of the couple **4**/**4**$^+$ and **5b**/**5b**$^+$ are now available.

---

* To whom correspondence should be addressed. E-mail: zanello@unisi.it (P.Z.), pjb@ch.pw.edu.pl (P.B.).

[†] Università di Siena.

[‡] Warsaw University of Technology.

[§] Polish Academy of Sciences of Warsaw.

[||] University of Wrocaw.

(1) Douglas, W. E. *J. Chem. Soc., Dalton Trans.* **2000**, 57.

(2) Kelly, R. A., III; Scott, N. M.; Diez-Gonzales, S.; Stevens, E. D.; Nolan, S. P. *Organometallics* **2005**, *24*, 3442.

(3) Buchowicz, W.; Kozio, A.; Jerzykiewicz, L. B.; Lis, T.; Pasynkiewicz, S.; Pêcherzewska, A.; Pietrzykowski, A. *J. Mol. Catal., A: Chem.* **2006**, *257*, 118.

10.1021/ic701226d CCC: $37.00

Chart 1

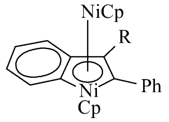

R = Me (**1**)

R = Et (**2**)

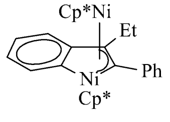

3

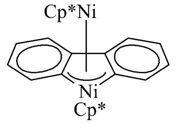

4

Chart 2

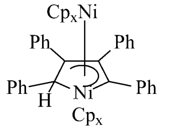

$Cp_x = Cp = C_5H_5$ **5a**

$Cp_x = Cp' = C_5H_4CH_3$ **5b**

Experimental Section

All reactions were carried out in an atmosphere of dry argon or nitrogen using Schlenk tube techniques. Solvents were dried by conventional methods. ^1H and ^{13}C NMR spectra were measured on a Varian Mercury 400BB instrument. Electron impact mass spectra were recorded on an AMD-604 spectrometer. Electrospray mass spectra were recorded on Applied Biosystems 4000 QTRAP spectrometer. 1,4-Dilithio-1,2,3,4-tetraphenyl-1,3-butadiene (**6**) was synthesized according to the literature method.[8] The syntheses of **2**−**4** were described in previous papers.[6,7]

Electrochemical measurements were performed in deaerated, freshly distilled (from sodium benzophenone) THF solutions containing $[NBu_4][PF_6]$ (0.2 mol dm^{-3}) as supporting electrolyte (Fluka, electrochemical grade). Cyclic voltammetry was performed in a three electrode cell containing the working electrode surrounded by a platinum-spiral counter electrode and the reference electrode (SCE) mounted with a Luggin capillary.[9] Platinum or gold electrodes were used as working electrodes. A BAS 100W electrochemical analyzer was used as polarizing unit. All the potential values are referred to the saturated calomel electrode (SCE). Under the present experimental conditions, the one-electron oxidation of ferrocene occurs at +0.56 V ($\Delta E_p = 100$ mV at 0.1 V s^{-1}).

Controlled potential coulometry was performed in an H-shaped cell with anodic and cathodic compartments separated by a sintered-glass disk. The working macroelectrode was a platinum gauze; a mercury pool was used as the counter electrode.

UV−vis spectroelectrochemical measurements were carried out using a Perkin-Elmer Lambda 900 UV−vis spectrophotometer and an optically transparent thin-layer electrode cell (OTTLE cell) equipped with a Pt-minigrid working electrode (32 wires/cm), Pt minigrid auxiliary electrode, Ag wire pseudoreference, and CaF_2 windows.[10] During the microelectrolysis procedures, the electrode potential was controlled by an Amel potentiostat 2059 equipped with an Amel function generator 568. Nitrogen-saturated THF solutions of the compounds under study were used with $[NBu_4][PF_6]$ (0.2 mol dm^{-3}) as supporting electrolyte.

Electron spin resonance (ESR) spectra were recorded with a ER 200 D-SRC Bruker spectrometer operating at X-band frequencies using a HS Bruker rectangular cavity. The control of the operational frequency was obtained with a Hewlett-Packard X532B wavemeter, and the magnetic field was calibrated with the DPPH (1,1-diphenyl-2-picrylhydrazyl) radical as a suitable field marker. The temperature was controlled by a Bruker ER 4111 VT device (±1 K) and with an OxfordESR900 helium continuous-flow cryostat. The *g* values are referred to DPPH ($g = 2.0036$) used as an external standard reference.

Synthesis of 5a. A 1.194 g amount of **6** (2.3 mmol) and 40 cm^3 of diethyl ether were placed in Schlenk flask and cooled to −50 °C. The solution of nickelocene (0.889 g; 4.7 mmol) in 40 cm^3 of diethyl ether was slowly added. The reaction mixture was stirred for 1 h at −50 °C and then at room temperature overnight. The solvent was then removed, and the residue was extracted with toluene (2 × 80 cm^3). Extracts were filtered through a bed of alumina and concentrated to approximately 10 cm^3. Alumina was added and then dried. The products of the reaction, absorbed on alumina, were placed on the top of the column (neutral alumina deactivated with 5% of water) and chromatographed with hexane/toluene mixtures as eluents. Four colored bands were separated and collected.

The first green fraction (10:1 hexane−toluene) contained unreacted nickelocene. The second fraction (yield 0.153 g) contained a mixture of different, not properly identified organic and organometallic compounds. In the EIMS spectrum of this mixture there were molecular peaks which suggest the presence of one or two nickel atoms in the molecules.

The third brown fraction (4:1 hexane−toluene) gave solid **5a** (yield 0.209 g, 0.35 mmol, ca. 15%). EIMS (70 eV) *m*/*e* (rel int) (^{58}Ni): 603 (72%, M^+), 537 (99%, $C_{33}H_{25}Ni_2^+$), 479 (60%, $C_{33}H_{25}Ni^+$), 414 (58%, $C_{28}H_{20}Ni^+$), 267 (38%, $C_{21}H_{15}^+$), 188 ($C_{10}H_{10}Ni^+$), 123 (39%, $C_5H_5Ni^+$), 105 (100%, $C_8H_9^+$). EI HR MS: obsd *m*/*e* = 603.112 29; calcd for $C_{38}H_{31}{}^{58}Ni_2$ = 603.113 27.

The fourth violet fraction (1:1 hexane−toluene) gave solid **7a** (yield 0.101 g, 0.12 mmol, ca. 8%). ^1H NMR (C_6D_6) [δ (ppm)]: 6.72−8.25 (m, 30H, Ph), 5.16 (s, 5H, Cp), 4.78 (s, 5H, Cp). ^{13}C NMR (C_6D_6) [δ (ppm)]: 125−177 (Ph), 103.20 (C≡C), 95.34 (C≡C), 90.80 (Cp), 88.12 (Cp). EIMS (70 eV) *m*/*e* (rel int) (^{58}Ni): 838 (10%, M^+), 660 (16%, $C_{38}H_{30}Ni_3^+$), 602 (9%, $C_{34}H_{20}Ni_3^+$), 534 (100%, $C_{42}H_{30}^+$), 479 (26%, $C_{33}H_{25}Ni^+$), 414 (14%, $C_{28}H_{20}Ni^+$), 246 (12%, $C_{10}H_{10}Ni_2^+$), 188 (12%, $C_{10}H_{10}Ni^+$), 178 (20%, $C_{14}H_{10}^+$), 123 (14%, $C_5H_5Ni^+$). EI HR MS: obsd 838.117 36; calcd for

---

(4) See for example: (a) Baimbridge, C. W.; Dickson, R. S.; Fallon, G. D.; Grayson, I.; Nesbit, R. J.; Weigold, J. *Aust. J. Chem.* **1986**, *39*, 1187. (b) McGhee, W. D.; Bergman, R. G. *J. Am. Chem. Soc.* **1988**, *110*, 4246. (c) Sünkel, K. *J. Organomet. Chem.* **1990**, *391*, 247. (d) Perthuisot, C.; Edelbach, B. L.; Zubris, D. L.; Jones, W. D. *Organometallics* **1997**, *16*, 2016. (e) Luo, S.; Ogilvy, A. E.; Rauchfuss, T. B.; Rheingold, A. L.; Wilson, S. R. *Organometallics* **1991**, *10*, 1002. (f) Omori, H.; Suzuki, H.; Moro-oka, Y. *Organometallics* **1989**, *8*, 1576. (g) Suzuki, H.; Omori, H.; Lee, D. H.; Yoshida, Y.; Fukushima, M.; Tanaka, M.; Moro-oka, Y. *Organometallics* **1994**, *13*, 1129. (h) Campion, B. K.; Heyn, R. H.; Tilley, T. D. *Organometallics* **1990**, *9*, 1106. (i) Müller, J.; Akhnoukh, T.; Escarpa Gaede, P.; Ao-ling Guo; Moran, P.; Ke Qiao *J. Organomet. Chem.* **1997**, *541*, 207. (j) Brady, L. A.; Dyke, A. F.; Garner, S. E.; Knox, S. A. R.; Irving, A.; Nicholls, S. M.; Orpen, A. G. *J. Chem. Soc., Dalton Trans.* **1993**, 487. (k) Wadepohl, H.; Borchert, T.; Büchner, K.; Herrmann, M.; Paffen, F.-J.; Pritzkow, H. *Organometallics* **1995**, *14*, 3817. (l) Wadepohl, H.; Metz, A.; Pritzkow, H. *Chem.*−*Eur. J.* **2002**, *8*, 1591. (m) Nishio, M.; Matsuzaka, H.; Mizobe, Y.; Tanase, T.; Hidai, M. *Organometallics* **1994**, *13*, 4214.

(5) Buchalski, P.; Pietrzykowski, A.; Pasynkiewicz, S.; Jerzykiewicz, L. B. *J. Organomet. Chem.* **2005**, *690*, 1523.

(6) Buchalski, P.; Pasynkiewicz, S.; Pietrzykowski, A.; Pika, A.; Suwiñska, K. *Inorg. Chem. Commun.* **2006**, *9*, 375.

(7) Buchalski, P.; Kozio, A.; Pasynkiewicz, S.; Pietrzykowski, A.; Suwiñska, K.; Zdziemborska, M. *J. Organomet. Chem.* **2006**, *691*, 4080.

(8) Eish, J. J. *Organometallic Synthesis*; Academic Press: New York, 1981; p 98.

(9) Zanello, P. In *Inorganic electrochemistry. Theory, practice and application*; RSC: Oxford, U.K., 2003.

(10) Krejèik, M.; Danìk, M.; Hartl, F. *J. Electroanal. Chem.* **1991**, *317*, 179.

$C_{52}H_{40}{}^{58}Ni_3$ 838.119 04. These data are in agreement with the previously published values.[11]

Synthesis of 5b. The reaction was carried out as above using 1.316 g (2.54 mmol) of **6** in 70 cm^3 of diethyl ether and 1.071 g (4.96 mmol) of bis(methylcyclopentadienyl)nickel in 40 cm^3 of diethyl ether. Four colored bands were separated and collected.

The first two fractions contained unreacted bis(methylcyclopentadienyl)nickel and the mixture (yield 0.387 g) of different, not properly identified organic and organonickel compounds.

The third brown fraction (2:1 hexane−toluene) gave solid **5b** (yield 0.305 g, 0.48 mmol, ca. 19%). EIMS (70 eV) *m*/*e* (rel int) (^{58}Ni): 631 (89%, M$^+$), 551 (100%, $C_{34}H_{27}Ni_2{}^+$), 473 (33%, $C_{28}H_{21}Ni_2{}^+$), 414 (54%, $C_{28}H_{20}Ni^+$), 335 (13%, $C_{17}H_{15}Ni_2{}^+$), 276 (12%, $C_{17}H_{14}Ni^+$), 236 (15%, $C_{14}H_{10}Ni^+$), 178 (11%, $C_{14}H_{10}{}^+$), 136 (8%, $C_6H_6Ni^+$). EI HR MS: obsd 631.143 71; calcd for $C_{40}H_{35}{}^{58}Ni_2$ 631.144 57. Crystals of **5b** suitable for X-ray measurements were grown from hexane−THF solution.

The fourth violet fraction (1:1 hexane−toluene) gave solid **7b** (yield 0.18 g, 0.09 mmol, ca. 13%). ^{1}H NMR (C_6D_6) [δ (ppm)]: 6.70−8.20 (m, 30H, Ph), 5.18 (m, 2H, CH (Cp′)), 5.04 (m, 2H, CH (Cp′)), 4.72 (m, 2H, CH (Cp′)), 4.63 (m, 2H, CH (Cp′)), 1.33 (s, 3H, CH$_3$), 1.18 (s, 3H, CH$_3$). ^{13}C NMR (C_6D_6) [δ (ppm)]: 125−177 (Ph), 107.59 (C≡C), 104.22 (C≡C), 102.29 (C≡C), 95.64 (CH), 94.86 (CH), 91.28 (CH), 90.19 (CH), 12.58 (CH$_3$), 11.57 (CH$_3$). EIMS (70 eV) *m*/*e* (rel int) (^{58}Ni): 866 (46%, M$^+$), 688 (84%, $C_{40}H_{34}Ni_3{}^+$), 608 (34%, $C_{34}H_{26}Ni_3{}^+$), 551 (40%, $C_{34}H_{27}Ni_2{}^+$), 493 (58%, $C_{34}H_{27}Ni^+$), 414 (64%, $C_{28}H_{20}Ni^+$), 267 (41%, $C_{21}H_{15}{}^+$), 236 (37%, $C_{14}H_{10}Ni^+$), 178 (91%, $C_{14}H_{10}{}^+$), 136 (19%, $C_6H_6Ni^+$). EI HR MS: obsd 866.149 12; calcd for $C_{54}H_{44}{}^{58}Ni_3$ 866.150 34.

Oxidation of 4 with $[Cp_2Fe]^+PF_6{}^-$. A 0.293 g amount of **4** (0.54 mmol) was reacted with $[Cp_2Fe]^+PF_6{}^-$ (0.178 g; 0.54 mmol) in 30 cm^3 of dichloromethane at room temperature for 24 h. The resulting green solution was filtered and concentrated to 15 cm^3. A 50 cm^3 volume of diethyl ether was then added, and a black solid was precipitated. It was washed three times with diethyl ether and dried (yield: 0.211 g; 0.31 mmol; 57%). The solid was dissolved in dichloromethane, and diethyl ether was layered over the solution. After 2 days black crystals of $\mathbf{4^+PF_6{}^-}$, suitable for X-ray measurements, were formed. ^{1}H NMR (CD_2Cl_2) (30 °C) [δ (ppm)]: 102.42 (s, 2H), 62.03 (s, 30H, Cp*), 9.90 (s, 2H, Ar), −6.13 (s, 2H, Ar), −21.43 (s, 2H, Ar), −40.49 (s, 2H, Ar). ^{19}F NMR ($CDCl_3$) (20 °C) [δ (ppm)]: −75.62, −77.51. ^{31}P NMR ($CDCl_3$) (20 °C) [δ (ppm)]: −143.81. Electrospray MS (acetone) *m*/*e* (^{58}Ni): 538 (**4**$^+$), 145 ($PF_6{}^-$).

Oxidation of 5b with $[Cp_2Fe]^+PF_6{}^-$. The reaction was carried out as above using 0.254 g (0.4 mmol) of **5b** and 0.131 g (0.4 mmol) of $[Cp_2Fe]^+PF_6{}^-$ in 40 cm^3 of dichloromethane. The yield of a crude product was 0.206 g (0.27 mmol, 67%). It was then dissolved in dichloromethane, and diethyl ether was layered over the solution. After 1 day black crystals of $\mathbf{5b^+PF_6{}^-}$, suitable for X-ray measurements, were formed. ^{1}H NMR (acetone-*d*$_6$) (20 °C) [δ (ppm)]: 7.05−8.14 (m, 20H, Ph), 6.60 (m, 1H, Cp′), 6.22 (m, 2H, Cp′), 6.12 (m, 1H, Cp′), 5.86 (m, 1H, Cp′), 5.80 (m, 1H, Cp′), 5.71 (s, 1H, CH), 4.64 (m, 1H, Cp′), 4.24 (m, 1H, Cp′), 1.49 (s, 3H, CH$_3$), 0.83 (s, 3H, CH$_3$). ^{13}C NMR (acetone-*d*$_6$) (20 °C) [δ (ppm)]: 184.2, 136.9, 133.6, 132.7, 131.5, 130.7, 130.6, 130.0, 129.5, 129.2, 127.4, 126.9, 123.1, 116.1, 113.6, 104.2, 103.9, 103.1, 101.3, 99.3, 94.1, 93.6, 91.8, 90.8, 54.9, 45.3, 10.7, 10.5. Electrospray MS (acetone) *m*/*e* (^{58}Ni): 631 (**5b**$^+$), 145 ($PF_6{}^-$).

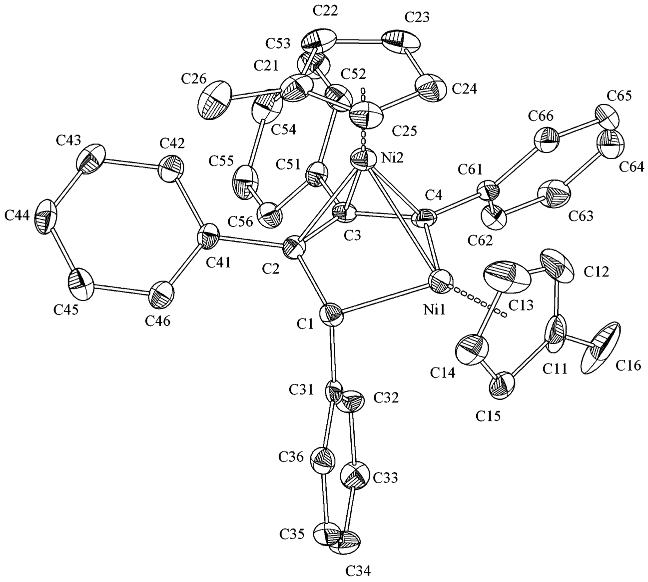

Figure 1. ORTEP view of the molecular structure of **5b** showing the atom-numbering scheme. Thermal ellipsoids are drawn at the 50% probability level.

X-ray Structure Determination of 5b. Preliminary examination and intensities data collections were carried out on a KUMA KM4 κ-axis diffractometer with graphite-monochromated Mo Kα radiation and with a CCD camera. All data were corrected for Lorentz, polarization, and absorption effects. Data reduction and analysis were carried out with the Oxford Diffraction programs.[12] The structure was solved by direct methods and refined by the full-matrix least-squares method on all F^2 data using the SHELXTL_NT V5.1 software.[13] Carbon-bonded hydrogen atoms were included in calculated positions and refined in the riding mode using SHELXL97 default parameters. Other hydrogen atoms were located in a difference map and refined isotropically without any restrains. All non-hydrogen atoms were refined with anisotropic displacement parameters. The molecular structure of **5b** is presented in Figure 1, and selected interatomic distances are given in Table 2. Crystal data, data collection, and refinement parameters for **5b** are given in Table 1.

X-ray Structure Determination of $4^+PF_6{}^-$ and $5b^+PF_6{}^-$. The crystals were sealed in a glass capillary under a nitrogen stream. The diffractometer control program Collect was used;[14] the unit cell parameters and the data reduction were treated according to Denzo and Scalepak.[15] The structures were solved by direct methods SHELXS-97[16] and refined on F^2 by full-matrix least squares with SHELXL-97.[17] All the hydrogen atoms were placed in calculated positions and refined using a riding model.

Molecular structures of $\mathbf{4^+PF_6{}^-}$ and $\mathbf{5b^+PF_6{}^-}$ are presented in Figures 2 and 4, respectively, and selected interatomic distances are given in Table 3. Crystal data, data collection, and refinement parameters for complexes $\mathbf{4^+PF_6{}^-}$ and $\mathbf{5b^+PF_6{}^-}$ are given in Table 1.

---

(11) Pasynkiewicz, S.; Pietrzykowski, A.; Kryza-Niemiec, B.; Zachara, J. *J. Organomet. Chem.* **1998**, *566*, 217.

(12) *Oxford Diffration Software*, version 1.171.13; Oxford Diffration Ltd.: Abingdon, Oxfordshire, England, 2003.

(13) Sheldrick, G. M. *SHELXTL*, version 5.10; Bruker AXS Inc.: Madison, WI, 1997.

(14) *"Collect" data collection software*; Nonius, BV: Delft, The Netherlands, 1998.

(15) Otwinowski, Z.; Minor, W. Processing of X-ray Diffraction Data Collected in Oscillation Mode. In *Methods in Enzymology*; Carter, C. W., Jr., Sweet, R. M., Eds.; Academic Press: New York, 1997; Vol. 276, Macromolecular Crystallography, Part A, pp 307−326.

(16) Sheldrick, G. M. SHELXS-97. *Acta Crystallogr., Sect. A* **1990**, *46*, 467.

(17) Sheldrick, G. M. *SHELXL-97, Program for the refinement of crystal structures*; University of Göttingen: Göttingen, Germany, 1997.

Table 1. Crystal Data and Structure Refinement Parameters for Complexes **5b**, **5b$^+$PF$_6$$^-$**, and **4$^+PF_6$$^-$**

param	**5b**	**5b$^+$PF6$^-$**	**4$^+$PF$_6$$^-$**
empirical formula	$C_{40}H_{35}Ni_2$	$C_{41}H_{37}Cl_2F_6Ni_2P$	$C_{32}H_{38}F_6Ni_2P$
cryst size (mm)	0.12 × 0.09 × 0.06	0.40 × 0.16 × 0.08	0.08 × 0.04 × 0.04
cryst system	orthorhombic	triclinic	orthorhombic
space group	$P2_12_12_1$	$P\bar{1}$	*Pbca*
unit cell dimens (Å, deg)	$a = 11.102(3)$ $b = 15.165(3)$ $c = 17.955(4)$	$a = 9.5894(3)$ $b = 10.4044(3)$ $c = 18.4060(6)$ $\alpha = 93.368(2)$ $\beta = 98.260(2)$ $\gamma = 92.032(2)$	$a = 14.8268(4)$ $b = 13.7922(5)$ $c = 29.054(1)$
V (Å^3)	3022.9(12)	1812.4 (1)	5941.4(3)
Z	4	2	8
fw	633.10	863.00	685.01
D(calcd) (Mg·m^{-3})	1.391	1.581	1.532
temp (K)	100(2)	100(2)	100(2)
abs coeff (mm^{-1})	1.273	1.292	1.380
F(000)	1324	884	2840
λ(Mo Kα radiatn) (Å)	0.710 73 (graphite monochromator)	0.710 73 (graphite monochromator)	0.71073 (graphite monochromator)
θ range for data collcn (deg)	2.92−29.07	2.97−27.43	2.91−21.97
scan type	$\omega-2\theta$	$\omega-2\theta$	$\omega-2\theta$
index ranges	$-15 \le h \le 15, -20 \le k \le 20, -24 \le l \le 22$	$-12 \le h \le 12, -12 \le k \le 13, -23 \le l \le 23$	$-15 \le h \le 15, -14 \le k \le 14, -30 \le l \le 30$
reflcns collcd/unique	41 854/8004 [$R_{int} = 0.0836$]	27 424/8050 [$R_{int} = 0.091$]	23 625/3620 [$R_{int} = 0.081$]
refinement method	full-matrix least squares on F^2	full-matrix least squares on F^2	full-matrix least squares on F^2
data/restraints/params	8004/0/385	8050/0/472	3620/0/369
goodness-of-fit on F^2	0.933	1.11	1.23
final R indices [$I > 2\sigma(I)$]			
$R_1 = \Sigma(F_o - F_c)/\Sigma F_o$	$R_1 = 0.0425$	$R_1 = 0.059$	$R_1 = 0.105$
$wR_2 = \{\Sigma[w(F_0^2 - F_c^2)^2]/\Sigma[w(F_o^2)^2]\}^{1/2}$	wR_2 (refined) = 0.0577	wR_2 (refined) = 0.112	wR_2 (refined) = 0.213
weighting scheme,[a]	$a = 0.0222$	$a = 0.0000$	$a = 0.0000$
where $P = (F_o^2 + 2F_c^2)/3$	$b = 0.0000$	$b = 6.0152$	$b = 99.0716$
R indices (all data)	$R_1 = 0.0714$, $wR_2 = 0.0619$	$R_1 = 0.080$, $wR_2 = 0.1120$	$R_1 = 0.140$, $wR_2 = 0.226$
largest diff peak and hole (e·Å^{-3})	0.302 and −0.308	0.543 and −0.732	0.680 and −0.543

[a] $w^{-1} = \sigma^2(F_o^2) + (aP)^2 + bP$.

Results and Discussion

Synthesis and Structures of 5a,b. The present nickelacyclic analogues of nickelocene have been prepared by reaction of 1,4-dilithio-1,2,3,4-tetraphenyl-1,3-butadiene (**6**) with 2 equiv of the proper nickelocene in diethyl ether at −50 °C. After warming up to room temperature, the reaction mixture was separated by column chromatography on neutral alumina.

Although the separation of all products was not possible, the new dinuclear nickelacyclic **5a** was isolated (eq 1).

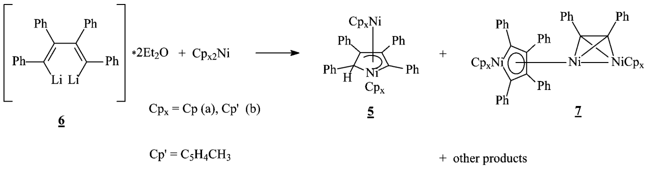

5a is paramagnetic with one unpaired electron/molecule (see the EPR spectroscopy in the pertinent section). The ^{1}H NMR spectrum does not exhibit any signal in the range from 0 to 10 ppm. EI MS spectrum shows the molecular peak at $m/e = 603$ with the isotopic pattern characteristic for two nickel atoms. This was confirmed by the HR EI MS $m/e = 603.112\,29$ which well-fitted the formula $C_{38}H_{31}Ni_2$. Even if we were unable to grow crystals suitable for X-ray measurements, it seems plausible to assume that its structure is similar to that below discussed for **5b**.

Table 2. Selected Interatomic Distances (Å) and Angles (deg) for **5b** and **5b$^+$PF$_6$$^-$**

param	**5b**	**5b$^+$PF6$^-$**
Ni1−Ni2	2.486(1)	2.379(1)
Ni1−C1	1.976(3)	1.984(4)
Ni1−C4	1.903(2)	1.915(4)
{Ni2−C1}	{2.727(3)}	{2.689(4)}
Ni2−C2	2.085(3)	2.093(4)
Ni2−C3	2.027(2)	2.034(4)
Ni2−C4	1.997(3)	1.979(4)
C1−C2	1.504(4)	1.494(5)
C2−C3	1.439(3)	1.431(5)
C3−C4	1.430(3)	1.435(5)
Ni2−Ni1−Cg	140.18(2)	141.66(3)
Ni1−Ni2−Cg	130.94(2)	129.91(3)
C1−Ni1−C4	85.6(1)	85.9(2)
Ni1−C1−C2	103.9(2)	103.0(2)
Ni1−Ni2−C2	73.5(1)	75.2(1)

5b was obtained in 20% yield under the same conditions as **5a**. EI MS and HR EI MS spectra confirmed the formula $C_{40}H_{35}Ni_2$. Crystals suitable for X-ray measurements were grown from hexane/THF solution. **5b** crystallizes in an orthorhombic crystal system. Its molecular structure is presented in Figure 1, and selected interatomic distances and angles are shown in Table 2.

The four carbon atoms C1−C4 and the Ni1 atom form a five-membered metallacyclic ring, which is not planar but exhibits an "open envelope" conformation. The three carbon atoms C2−C4 and the Ni1 atom are situated in one plane while the C1 atom is deviated by 0.544 Å from this plane in a direction opposite to the Ni2 atom. In turn, the Ni2 atom is bonded to the four atoms C2−C4 and Ni1 of the

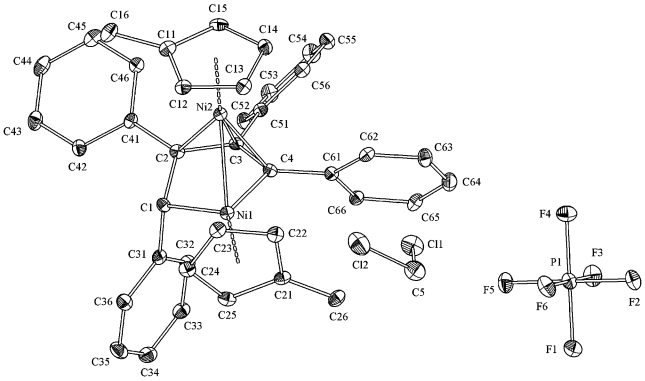

Figure 2. ORTEP view of the molecular structure of $\mathbf{5b^+PF_6^-}$ showing the atom-numbering scheme. Thermal ellipsoids are drawn at the 30% probability level.

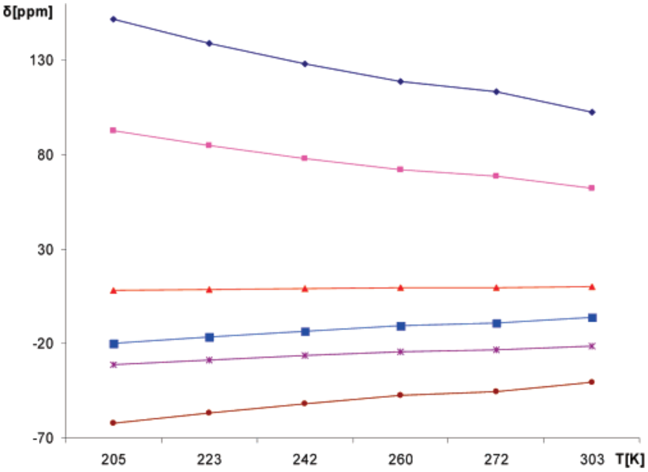

Figure 3. Temperature dependence of the ^{1}H NMR chemical shifts in $\mathbf{4^+PF_6^-}$.

nickelacyclic ring. The Ni1−Ni2 distance although long (2.49 Å) is still within the range of a nickel−nickel single bond.

The nickelacyclic ring can be described as a nickelacyclopentenyl ring, in that it arises from the replacement of one lithium atom of **6** by an hydrogen atom, the source of which is unknown. It is noted that a similar reaction of Cp*Ni(acac) with 1,4-dilithio-1,2,3,4-tetraphenyl-1,3-butadiene (**6**) afforded the mononuclear complex Cp*Ni(η^1,η^2-C_4HPh_4), in which the Ni(η^1,η^2-C_4HPh_4) ring is isomeric to the nickelacyclic ring of **5** [which can be described as Ni(η^1,η^1-C_4HPh_4)].[18] In fact, analysis of MS spectra of the mixture of the other products generated in the reaction indicated that small amounts of the mononuclear complexes CpNi(η^1,η^2-C_4HPh_4) and Cp'Ni(η^1,η^2-C_4HPh_4) were also formed.

Examination of the bond lengths of **5b** might lead to the conclusion that the bonding mode of the Ni2 atom to the nickelacyclic ring could be described as η^1,η^3; however, a substantial shortening of the Ni1−C4 bond (1.903(2) Å) in comparison with the single Ni1−C1 bond (1.976(3) Å) suggests that the bonding mode can be regarded as η^4 (through the atoms C2−C4 and Ni2). Thus, **5b** would be the first example in which a five-membered nickelacyclic ring is bonded to another metal atom in a η^4 manner.

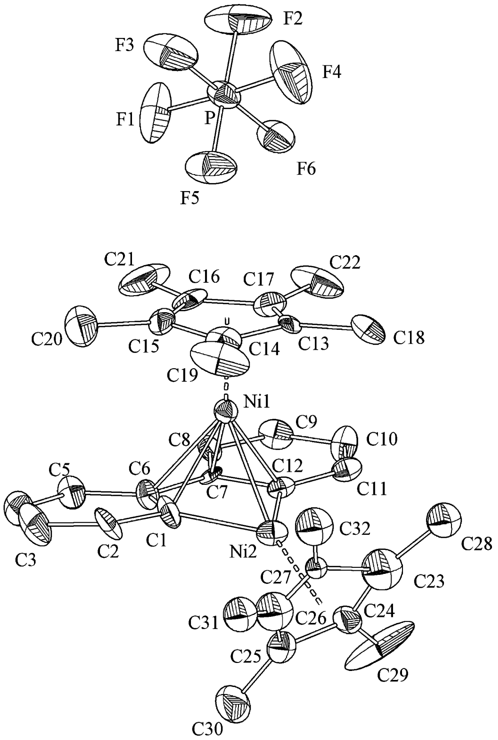

Figure 4. ORTEP view of the molecular structure of $\mathbf{4^+PF_6^-}$ showing the atom-numbering scheme. Thermal ellipsoids are drawn at the 40% probability level.

Table 3. Selected Interatomic Distances (Å) and Angles (deg) for $\mathbf{4^+PF_6^-}$ and **4**

param	$\mathbf{4^+PF6^-}$	$\mathbf{4}^a$
Ni1−Ni2	2.407(2)	2.400(1), 2.391(1)
Ni1−C1	2.11(1)	2.162(3), 2.162(3)
Ni1−C6	2.29(1)	2.415(3), 2.486(3)
Ni1−C7	2.17(1)	2.415(3), 2.486(3)
Ni1−C12	2.06(1)	2.162(3), 2.162(3)
Ni2−C1	1.91(1)	1.922(3), 1.932(3)
Ni2−C12	1.91(1)	1.922(3), 1.932(3)
Cg−Ni2−Ni1	160.3(1)	152.47(3), 152.39(3)
Ni2−Ni1−Cg	144.1(1)	151.35(3), 152.39(3)
C1−Ni2−C12	83.7(6)	84.1(2), 84.1(2)

^{a} Values for two independent molecules.[7]

Chemical Oxidation of 5b and 4. On the basis of the electrochemical findings below discussed, $[Cp_2Fe]^+PF_6^-$ was judged as a proper oxidant to prepare the monocations $\mathbf{5b^+PF_6^-}$ and $\mathbf{4^+PF_6^-}$.

5b reacts with $[Cp_2Fe]^+PF_6^-$ in dichloromethane to give the dark-green, diamagnetic, solid $\mathbf{5b^+PF_6^-}$, which was characterized by ^{1}H NMR and ^{13}C NMR spectroscopy.

Crystals of $\mathbf{5b^+PF_6^-}$ appropriate for X-ray diffraction studies were grown from dichloromethane−diethyl ether solution. It crystallizes in a triclinic crystal system. The molecular structure of the cation $\mathbf{5b^+}$, Figure 2, is similar to that of the parent **5b**, and selected interatomic distances and angles are shown in Table 2. The striking feature is the substantial shortening of the Ni1−Ni2 bond by 0.11 Å on passing from **5b** to $\mathbf{5b^+}$. The other bonds differ by no more than 2 ESDs.

---

(18) Denniger, U.; Schneider, J. J.; Wilke, G.; Goddard, R.; Krömer, R.; Krüger, C. *J. Organomet. Chem.* **1993**, *459*, 349.

Compound **4** reacted with $[Cp_2Fe]^+PF_6^-$ in dichloromethane to give the dark-green, paramagnetic, solid $\mathbf{4^+PF_6^-}$. Contrary to **4**, which showed only four broad signals of very low intensity, the room-temperature ^1H NMR spectrum of $\mathbf{4^+PF_6^-}$ shows six resonances at 102.42, 62.03, 9.90, −6.13, −21.43, and −40.49 ppm, respectively, the origin of one more signal (probably that at 102 ppm) being difficult to explain. The ^1H NMR spectrum depends reversibly from the temperature. As shown in Figure 3, the chemical shifts move toward the diamagnetic region of the spectrum as the temperature increases. The sharpening of the resonance lines upon warming indicates the shift toward diamagnetism and is consistent with two close-lying orbitals.

Crystals of $\mathbf{4^+PF_6^-}$ appropriate for X-ray diffraction studies were grown from dichloromethane−diethyl ether solution. The molecular structure is presented in Figure 4.

The compound crystallizes in an orthorhombic crystal system. Selected bond lengths and angles are compiled in Table 3 together with the corresponding bonds and angles in **4.**[7] The Ni1−Ni2 distance (2.41 Å) is typical for a nickel−nickel single bond.[5−7,11] The four carbon atoms C1, C6, C7, and C12 and the Ni2 atom form a five-membered metallacyclic ring. This ring is not planar but exhibits an “open envelope” conformation; in fact the four carbon atoms are situated in one plane while the nickel atom is deviated by 0.309 Å from this plane. The hinge angle, defined as the dihedral angle between the planes C1−C6−C7−C12 and C1−Ni2−C12, is 12.7°.

To define a bonding mode of the apical Ni1 atom to the nickelafluorenyl ring, we have determined the degree of slip-fold distortion, using the parameters described in ref 19. The slip parameter Δ_{M-C}, i.e. the difference between the average Ni1−C distances to C6 and C7 and those to C1 and C12, is ca. 0.14 Å, which indicates that the bonding mode of Ni1 to the nickelacyclic ring in $\mathbf{4}^+$ is η^5. This differs from **4**, in which the bonding mode of the central nickel atom to the nickelafluorenyl ring looks like intermediate between η^3 and η^5 (Δ_{M-C} = 0.32 Å and 0.25 Å in the two independent molecules).[7]

Electrochemistry. As illustrated in Figure 5, **2** undergoes in THF solution two oxidations and two reductions, all having features of chemical reversibility in the cyclic voltammetric time scale but for the most cathodic step.

Controlled-potential coulometry in correspondence of the first anodic process (E_w = +0.4 V) consumed one electron/molecule. As a consequence of the exhaustive electron removal, the original brown solution turns olive green, and in confirmation of the chemical reversibility of the passage $\mathbf{2}/\mathbf{2}^+$ in the long times of macroelectrolysis, the final solution displays a cyclic voltammetric profile quite complementary to the original one. The result further improves the time scale of the chemical reversibility deduced from cyclic voltammetric analysis in the scan rate range from 0.02 to 2.00 V s^{-1}, which is diagnostic for a simple one-electron oxidation ($i_{pa}\cdot v^{-1/2}$ substantially constant; i_{pc}/i_{pa} constantly equal to the unity) possessing substantial electrochemical reversibility (ΔE_p slightly higher that the theoretical value of 57 mV).[9]

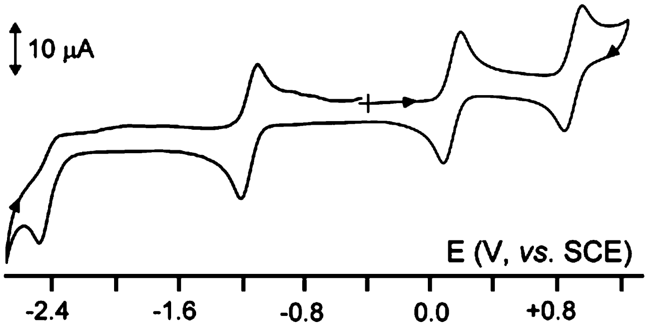

Figure 5. Cyclic voltammogram recorded at a gold electrode in THF solution of **2** (1.1×10^{-3} mol dm^{-3}). [NBu$_4$][PF$_6$] (0.2 mol dm^{-3}) is the supporting electrolyte. Scan rate: 0.2 V s^{-1}.

Similar electrochemical parameters are exhibited by the first reduction process, even if in the long times of macroelectrolysis (E_w = −1.5 V) the electrogenerated monoanion is only partially stable.

On the basis of the relative peak heights, we assume that either the most anodic or the most cathodic steps also involve one-electron processes. As a matter of fact, the most cathodic peak does not exhibit any directly associated reoxidation peak even at the highest scan rates, whereas the most anodic process presents features of partial chemical reversibility.

A qualitatively similar electron transfer ability is displayed by **3** and **4**, although the presence of the permethylated cyclopentadienyl ring, causing a general shift of all the processes toward more negative potentials, makes the most cathodic reduction to be obscured by the solvent discharge. In addition, because of hardly accountable electronic effects, the chemical stability of the different redox intermediates in the cyclic voltammetric time scale results slightly compromised ($i_{p(reverse)}/i_{p(direct)} < 1$).

A different behavior is exhibited by **5a**,**b**. In fact, as illustrated in Figure 6 for **5b**, they exhibit a one-electron oxidation as well as a one-electron reduction, both possessing features of chemical reversibility in the cyclic voltammetric time scale ($i_{p(reverse)}/i_{p(direct)}$ constantly equal to 1). A further, second oxidation occurs at high potential values very close to the solvent discharge.

Upon exhaustive one-electron oxidation (E_w = +0.5 V) the original orange-brown solution of **5b** turns green-brown and the resulting solution displays a cyclic voltammetric response complementary to the original one.

According to a classical viewpoint, the oxidation states of the nickel ions in **2**−**4** can be regarded as +2. In fact, substituting the CH$^+$ fragment by the isolobal $[CpNi^{II}]^+$,[21] one obtains the anionic $[(CpNi)C_4R_4]^-$ nickelacycle ring, in which the apical (sandwiched) nickel ion maintains the same oxidation number than in nickelocene (i.e., +2). On this

---

[19] Westcott, S. A.; Kakkar, A. K; Stringer, G.; Taylor, N.; Marder, T. B. *J. Organomet. Chem.* **1990**, *394*, 777.

[20] (a) Elian, M.; Hoffmann, R. *Inorg. Chem.* **1975**, *14*, 1058. (b) Elian, M.; Chen, M. M. L.; Mingos, D. M. P.; Hoffmann, R. *Inorg. Chem.* **1976**, 15, 1148. (c) Albright, T. A.; Burdett, J. K.; Whangbo, M-H. In *Orbital Interactions in Chemistry*; John Wiley & Sons: New York, 1985.

[21] King, M.; Holt, E. M.; Radnla, P., P.; McKennis, J. S. *Organometallics* **1982**, *1*, 1718.

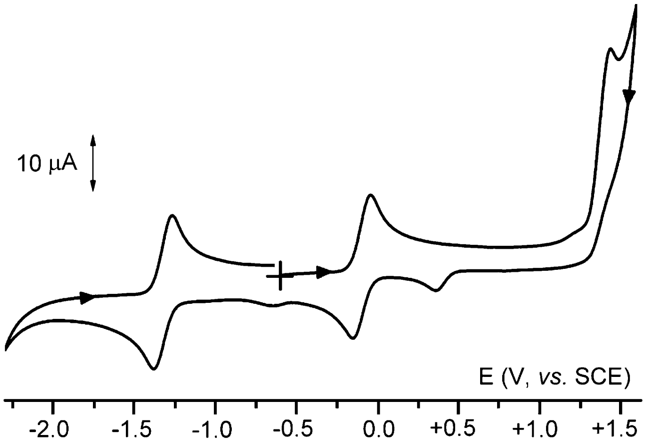

Figure 6. Cyclic voltammogram recorded at a gold electrode in THF solution of **5b** (0.9×10^{-3} mol dm^{-3}). $[NBu_4][PF_6]$ (0.2 mol dm^{-3}) is the supporting electrolyte. Scan rate: 0.2 V s^{-1}.

basis, we can assign the global charge 4+ to the $\{Ni_2\}$ couple in **2**−**4**. Accordingly, **2** exhibits a redox aptitude quite similar to that of nickelocene (which undergoes either the anodic sequence Ni(II)/Ni(III)/Ni(IV) or the cathodic Ni(II)/Ni(I) process).[22] This means that the two sequential oxidations can be considered as formally centered on the apical Ni(II) site, whereas the "relatively easy" first reduction of **2** could be formally assigned to the Ni(II)/Ni(I) reduction of the nickelacycle Ni(II) ion, as indirectly supported by the behavior of the nickelacycle complex $CpFe[NiC_4Ph_4]$, which exhibits a (unassigned) irreversible reduction at −1.24 V (vs SCE), in acetone solution.[23] In confirmation, the electrode potentials of the different redox changes exhibited by **2** are quite compatible with those of nickelocene, Table 4.

The situation is less straightforward for **5a**,**b**. In fact, the presence of an sp^3 carbon atom in the ring disrupts the aromatic character so that one of the five remaining electrons of the π system is driven toward the more electron withdrawing region, i.e., toward the nickel ion. In this case we assign the global charge 3+ to the $\{Ni_2\}$ couple, and in a first approximation, we attribute the oxidation state +1 to the basal nickel ion of the nickelacycle radical anion $[(CpNi)C_4R_4H]^{\bullet-}$, while the oxidation state of the apical Ni ion remains unchanged. On this basis, we tentatively assign the first oxidation of **5a**,**b** to the reversible Ni(I)/Ni(II) process of the Ni(I)-nickelacycle unit, whereas the Ni(II)/Ni(I) reduction and the almost overlapping solvent discharge Ni(II)/Ni(III) oxidation would be centered on the Ni(II) apical atom.

As shown in Table 5, with respect to the electron-transfer processes of **2**−**4**, the corresponding processes for **5a**,**b** display a general shift toward more anodic potential values, thus causing the Ni(III)/Ni(IV) of the apical nickel atom to be quite obscured by the solvent discharge.

Such an effect could be in part due to the electron-withdrawing effects of the phenyl substituents present in the basal ring, but as it will be discussed in the following section, it is likely that it is mainly due to the interruption of the aromaticity of the nickelacycle ring.

Obviously, the present formalism about the oxidation states of the nickel centers considers the electrons as completely localized. As a matter of fact, as we will discuss below, in all the complexes the Ni−Ni bond might deserve a more delocalized description.

Extended Hückel Insight into the Oxidation States of the Nickel Centers. In spite of the apparent successful analogy between nickelocene and **2**, the direct Ni−Ni interaction makes it too naive to conclude that the apical and basal Ni centers act as independent valence sites. In the attempt to throw further light into the electronic structure of the present complexes, an extended Hückel study was carried out. In particular, a fragment analysis was performed for nickelocene and for the simplified models of **2** and **5a** (in which the substituents of the nickelacycle ring have been replaced by hydrogen atoms).

In consideration of the EPR features at liquid helium (see below), the orbitals of the nickela-nickelocene **2** have been populated by two unpaired electrons (also supported by the magnetic measurements of the related **3** and **4**).[7] A simplified interaction diagram is illustrated in Figure 7. The orbital interaction between the nickel ions and the cyclopentadienyl rings is always antibonding in the range of energy shown in this diagram; therefore, for the sake of simplicity, the π orbitals of the cyclopentadienyl rings are not explicitly drawn. The left side of the diagram sketches the degenerate SOMOs couple in nickelocene, arising from the antibonding interaction between the partially occupied d_{xz}/d_{yz} couple of Ni in the $[NiCp]^+$ fragment and the couple of π filled orbitals of the Cp^- ring. At the right side, the interaction of two properly oriented $[NiCp]^+$ fragments affords the four fragment orbitals a−d, which are in turn combined with the linker $[C_4H_4]^{2-}$. This allows us to check how the frontier orbitals are perturbed by the replacement of $[C_4H_4]^{2-}$ with $[C_4H_5]^{2-}$ (and the addition of the extra electron, as required by the pertinent electron counting).

Given the asymmetry of the bonding with the linker, the molecular orbitals of $[NiCp]_2[C_4H_4]$ (the model of **2**) and $[NiCp]_2[C_4H_5]$ (the model of **5a**) can be localized or delocalized depending upon their interaction with the π system. In $[NiCp]_2[C_4H_4]$, the highest SOMO remains localized on the apical Ni ion and it is substantially unperturbed with respect to that of the degenerate nickelocene SOMOs. On the other hand, in the lower SOMO there is a strong mixing between d_{yz} orbitals of the apical and basal Ni ions. Indeed, in this orbital the π system of $[C_4H_4]^{2-}$ interacts with the $d_{yz} - d_{yz}$ combination of the two nickel ions. Because of the better overlap between the basal Ni d_{yz} and the π system, this SOMO is slightly stabilized with respect to the degenerate set of SOMOs in nickelocene. Similarly, in the LUMO, the π system of $[C_4H_4]^{2-}$ has an antibonding interaction with the $d_{yz} + d_{yz}$ combination of the two nickel ions.

Formally, both the nickel ions in the $\{Ni_2\}^{4+}$ couple have a fractional oxidation state because the couple of delocalized orbitals contain a single electron, so that the $\{Ni_2\}^{4+}$ system

---

(22) Bard, A. J.; Garcia, E.; Kukharenko, S.; Strelets, V. V. *Inorg. Chem.* **1993**, *32*, 3528.

(23) Colbran, S. B.; Robinson, B. H.; Simpson, J. *Organometallics* **1985**, *4*, 1594.

Table 4. Formal Electrode Potentials (V vs SCE), Peak-to-Peak Separations (mV) (in Parentheses), and Current Ratios for the Changes in the Oxidation States of the Two Nickel Centers of **2**−**4** in THF Solution

	oxidn processes				redn processes			
complex	$E°'_{III/IV}$[a]	$i_{p(reverse)}/i_{p(direct)}$[b]	$E°'_{II/III}$[a]	$i_{p(reverse)}/i_{p(direct)}$[b]	$E°'_{II/I}$[c]	$i_{p(reverse)}/i_{p(direct)}$[b]	$E°'_{II/I}$[a]	$i_{p(reverse)}/i_{p(direct)}$[b]
2	+0.90 (94)[b]	0.8	+0.14 (86)[b]	1.0	−1.16 (91)[b]	1.0	−1.92[d]	
3	+0.54 (71)[b]	0.7	−0.24 (73)[b]	0.8	−1.50 (72)[b]	0.5	e	
4	+0.51 (89)[b]	0.9	−0.12 (85)[b]	0.9	−1.54 (76)[b]	0.7	e	
$Ni(C_5H_5)_2$	+0.96 (120)[b]	0.8	+0.12 (128)[b]	1.0	e		−1.77 (140)[b]	0.4

[a] Assumed to be centered on the apical Ni(II) atom. [b] Measured at 0.1 V s^{-1}. [c] Assumed to be centered on the nickelacycle Ni(II) atom. [d] Coupled to fast chemical complications. [e] Not detected.

Table 5. Formal Electrode Potentials (V vs SCE), Peak-to-Peak Separations (mV) (in Parentheses), and Current Ratios for the Changes in the Oxidation States of the Two Nickel Centers of **5a**,**b** in THF Solution

	oxidn processes				redn processes	
complex	$E°_{II/III}$[a]	$i_{p(reverse)}/i_{p(direct)}$[b]	$E°_{I/II}$[c]	$i_{p(reverse)}/i_{p(direct)}$[b]	$E°_{II/I}$[a]	$i_{p(reverse)}/i_{p(direct)}$[b]
5a	+1.42[b,d]		−0.02 (65)	1.0	−1.26 (67)	0.9
5b	+1.44[b,d]		−0.09 (90)	1.0	−1.31 (90)	1.0

[a] Assumed to be centered on the apical Ni(II) atom. [b] Measured at 0.1 V s^{-1}. [c] Assumed to be centered on the nickelacycle Ni(I) atom. [d] Coupled to fast chemical complications.

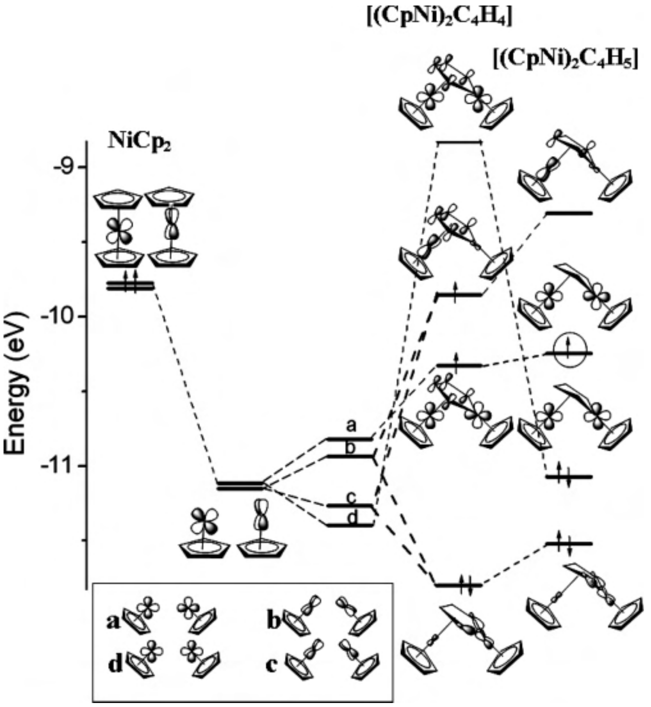

Figure 7. Generation the four fragment orbitals a−d from two properly oriented $[NiCp]^+$ fragments and their interaction with the $[C_4H_4]^{2-}$ or $[C_4H_5]^{2-}$ linkers (right). The interaction between the $[NiCp]^+$ fragment and the Cp^- ring to form nickelocene is also shown (left).

should be adequately represented as $\mathrm{Ni_{apical}^{2.5+}Ni_{basal}^{1.5+}}$. Moreover, even if the removal of one electron from complex **2** is a process close in energy with the removal of one electron from nickelocene, and it is also mainly centered on the apical nickel ion, it would correspond to the redox change $\mathrm{Ni_{apical}^{2.5+}Ni_{basal}^{1.5+} \rightarrow Ni_{apical}^{3.5+}Ni_{basal}^{1.5+}}$. On the other side, the addition of one electron (to the lower lying SOMO) should be easier in **2** than in nickelocene, as experimentally observed, and it should be centered on both the nickel ions, or $\mathrm{Ni_{apical}^{2.5+}Ni_{basal}^{1.5+} \rightarrow Ni_{apical}^{2+}Ni_{basal}^{1+}}$.

As far as complex $[NiCp]_2[C_4H_5]$ is concerned, the nonplanarity of the nickelacycle ring implies the dropping down of the $d_{yz} + d_{yz}$ combination of the two nickel ions (formerly giving rise to the LUMO in $[NiCp]_2[C_4H_4]$). As a consequence, the relative position of the localized and delocalized orbitals is now inverted. Since there is an extra electron, the nickel ions have again a fractional oxidation state because the HOMO and SOMO now are the couple of delocalized orbitals. Therefore, the formal charge in the $\{Ni_2\}^{3+}$ assembly should become $\mathrm{Ni_{apical}^{2.5+}Ni_{basal}^{0.5+}}$. This means that both the removal or addition of one electron from **5a** (and **5b**) are centered on both the nickel ions, thus corresponding to the redox changes $\mathrm{Ni_{apical}^{2.5+}Ni_{basal}^{0.5+} \rightarrow Ni_{apical}^{3+}Ni_{basal}^{1+}}$ and $\mathrm{Ni_{apical}^{2.5+}Ni_{basal}^{0.5+} \rightarrow Ni_{apical}^{2+}Ni_{basal}^{0}}$, respectively. According to the extended Hückel results, the oxidation of **5a**,**b** should be more difficult than that of nickelocene or **2**, even if the prediction does not fit the experimental data probably because of the inductive effects played by the different substituents.

In conclusion, the description of the present complexes through fractional oxidation states likely approaches their true electronic structure. It appears also evident that, due to the presence or the absence of an aromatic regime in the nickelacycle rings, a direct comparison of the redox pattern of **2**−**4** and **5a**,**b** is not easy.

Spectroelectrochemistry. Figure 8 shows the spectroelectrochemical trend recorded in a OTTLE cell upon progressive oxidation of **2** and **5b**, respectively. As far as the oxidation of **2** to $\mathbf{2}^+$ is concerned, a significant feature resides in the progressive appearance of a NIR band at about 940 nm, Figure 8a. In contrast, the NIR band of **5b** at about 920 nm progressively disappears upon oxidation, Figure 8b.

A plausible account for such a behavior can be deduced from Figure 9. The SOMO−LUMO transition in the **5b** model has the same nature of the hypothetical transition from the lower to the higher SOMOs in the **2** model, which however cannot be observed because it is spin-forbidden (Figure 9a). This latter becomes a spin-allowed SOMO−LUMO transition in the oxidized form $\mathbf{2}^+$, while it cannot be observed anymore in the depopulated $\mathbf{5b}^+$ (Figure 9b).

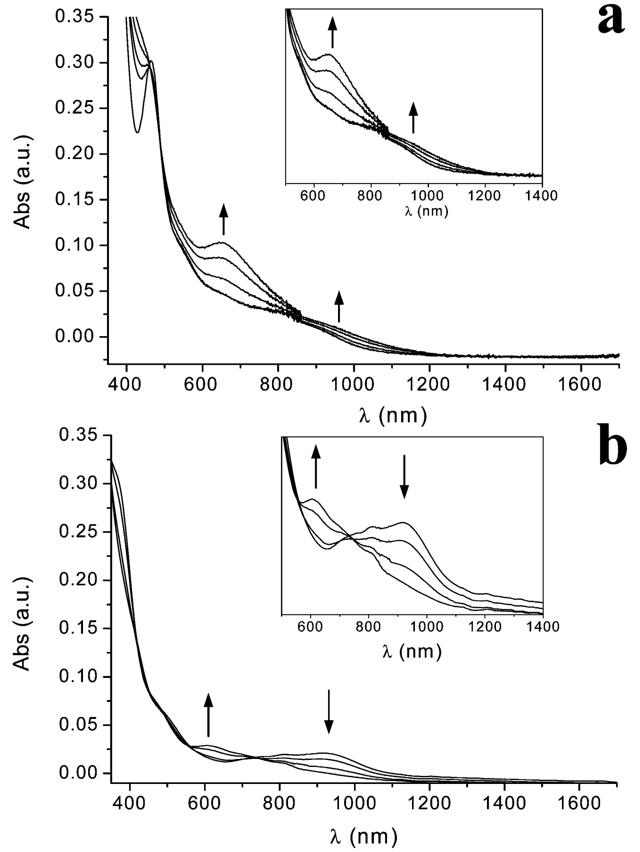

Figure 8. Spectroelectrochemical profiles recorded upon stepwise anodic oxidation of **2** (a) and **5b** (b) in THF solution.

In this picture, the NIR band would be due to the transition of an electron from a delocalized to a localized orbital and could be regarded as a partial $Ni_{basal} \rightarrow Ni_{apical}$ charge transfer.

EPR Spectroscopic Measurements. To throw further light on the nature of the above-discussed redox processes, EPR measurements have been carried out either on the original products or on their electrogenerated redox intermediates.

Let us start with **2**. In THF solution it is X-band EPR silent at liquid-nitrogen temperature (100 K), but in agreement with its solid-state magnetic moment (2.53 μ_B at $T = 298$ K), which preludes the presence of two unpaired electrons (total electron spin $S = 1$ in the ground state),[6] it resulted as EPR active at liquid-helium temperature, Figure 10.

The anisotropic rhombic line shape has been interpreted according to the electron spin Hamiltonian: $H_e = \beta{\cdot}H{\cdot}g{\cdot}S + S{\cdot}D{\cdot}S$ ($\beta{\cdot}H{\cdot}g{\cdot}S$, Zeeman contribution; $S{\cdot}D{\cdot}S$, zero field splitting contribution; D, traceless zero field splitting tensor (ZFS)).[24-26] The two signals in the low-field region (g) give evidence of the zero field splitting effect. In contrast, the medium- and high-field regions (g_m and g_h) overlap in two less resolved doublets. The anisotropic g_i and D_i parameters have been evaluated by multiple derivative line shape analysis, joined with simulation procedures, Table 6.[26,27] The pertinent g_i values clearly prove the metallic character imparted by the strong spin−orbit coupling.

No EPR evidence for hyperfine (hpf) ^{61}Ni ($I = 3/2$, natural abundance = 1.19%) or superhyperfine (shpf) ^{1}H, ^{13}C aromatic ligand interaction has been detected.

A weak and unresolved signal at low-field ($H_{averaged} = 1550(10)$ G; $g_{averaged} = 4.3(1)$, not shown in the Figure 10), which is attributed to the low-intensity forbidden $\Delta m_s = 2$ transition, confirms the $S = 1$ ground state of **2**.[24,25]

With an increase in the temperature, the anisotropic signal tends to disappear. Refreezing the solution at 4 K quantitatively recovers the rhombic spectrum.

In the solid state at 4.3 K, **2** affords 10 major absorptions at high magnetic field, as a consequence of the "spin−spin exchange" interaction among each randomly positioned paramagnetic microcrystallite ($S{\cdot}J{\cdot}S$ Hamiltonian).[24-26] An approximate g_h parameter can be evaluated through the intermediate H value of the spectral multiplet. The pertinent values are reported in Table 6, together with those of the other paramagnetic derivatives studied. In the low-field region two partially resolved intense signals and a very weak absorption ($H_{averaged} = 1580(40)$ G) are also detected, which are reminiscent of the related glassy solution spectrum.

The solid-state magnetic moment of 2.53 μ_B at 298 K preludes a $\langle g \rangle$ value of 1.79, while at 4.3 K the solid-state experimental $\langle g \rangle$ value is 2.11 (2.16 in frozen solution), which would correspond to a magnetic moment of 3.07 μ_B (2.98 μ_B in frozen solution). It is hence evident the active thermal effects on the ZFS and $S{\cdot}J{\cdot}S$ interactions.

Let us now pass to the X-band features of the electrogenerated monocation **2**$^+$, Figure 11.

The spectral analysis has been carried out on the basis of the Zeeman Hamiltonian, $H_e = \beta{\cdot}H{\cdot}g{\cdot}S$. The rhombic symmetry of the relatively narrow line shape ($g_i \neq g_e = 2.0023$) gives evidence to some metallic character of the unpaired electron. The $g_{l,m,h}$ features (see Table 6) well account for the spin−orbit coupling contribution to the anisotropic signals.

At the glassy-fluid transition a very narrow unresolved signal appears ($g_{iso} \approx \langle g \rangle$). Rapidly refreezing the solution quantitatively recovers the rhombic spectrum, indicating the chemical stability of the monocation.[24]

In conclusion, the X-band EPR features of **2** and **2**$^+$ agree with a theoretical $S = 1$ fundamental triplet state for the neutral complex and an $S = 1/2$ fundamental doublet state for the monocation, with temperature-dependent magnetic behaviors characterized by different electron spin relaxation mechanisms.[24-26]

In agreement with the partial chemical stability of **2**$^-$, in glassy solution its electrogeneration affords a series of low-intensity paramagnetic species spread on a very wide magnetic field.

---

(24) Mabbs, F. E.; Collison, D. Electron Paramagnetic Resonance of d Transition Metal Compounds. In *Studies in Inorganic Chemistry*; Elsevier: New York, 1992; Vol. 16.

(25) Drago R. S. *Physical Methods for Chemists*; Saunders College Publishing: New York, 1992.

(26) Carlin R. L. *Magnetochemistry*; Springer-Verlag: Berlin, 1986.

(27) (a) *XSophe Simulation Software*; Bruker ElectroSpin: Berlin, Germany. (b) Della Lunga, G. *ESRMGR Simulation Program Package*; Dept. of Chemistry, University of Siena: Siena, Italy, 1998.

Table 6. X-Band EPR Parameters of the Paramagnetic Species Examined under Different Experimental Conditions ($\delta_{l-h} = g_l - g_h$; l, Low-Field; m, Medium-Field; h, High-Field; g_i, ±0.008; D_i, ±5 G; $\langle g \rangle = 1/3(g_l + g_m + g_h)$; a_i, ΔH_i, ±3 G)

complex	g_l	g_m	g_h	$\langle g \rangle$	g_{iso}	D_l	D_m	D_h	δ_{l-h}
2[a,c]	2.209	2.068	2.039	2.105		28	36	12	0.170
2[b,c]	2.193	2.193	2.10[d]	2.16,[d] 1.789[e,f]		20	$\leq \Delta H_h$	$\leq \Delta H_h$	0.09
$\mathbf{2}^{+}$ [a,g]	2.080	2.021	1.909	2.003	2.004[e]				0.171
5a[a,g]	2.123	2.021	1.994	2.046	2.048[e]				0.129
5a[b,g]	2.083	2.033	2.014	2.043					0.069
5a[b,e]	2.086	2.036	2.020	2.047					0.066
5b[a,g]	2.119	2.019	1.992	2.043					0.127
5b[b,e]	2.094	2.040	2.004	2.046					0.094

[a] THF solution. [b] Solid state. [c] $T = 4.3$ K. [d] g_i: ±0.05. [e] $T = 298$ K. [f] Calculated from the solid-state magnetic moment at $T = 298$ K. [g] $T = 100$ K.

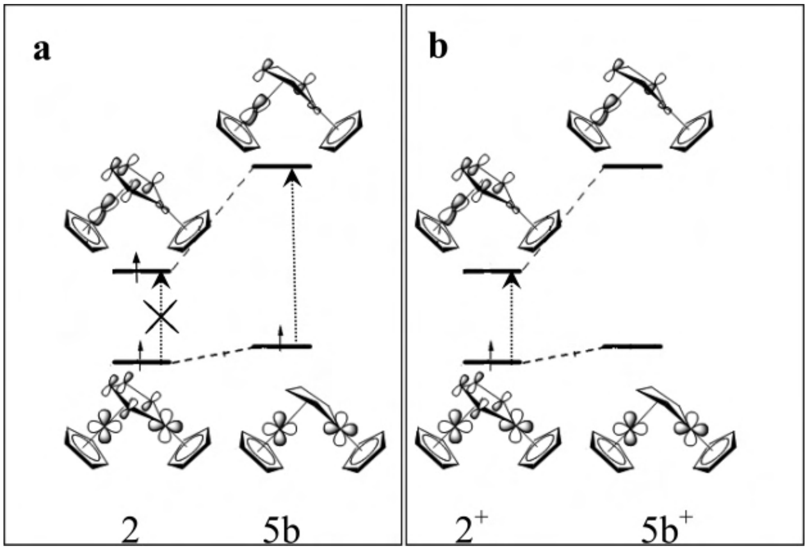

Figure 9. Hypothesis on the origin and trend of the NIR absorption in **2** and **5b** (a) and their cationic forms $\mathbf{2}^{+}$ and $\mathbf{5b}^{+}$ (b), respectively.

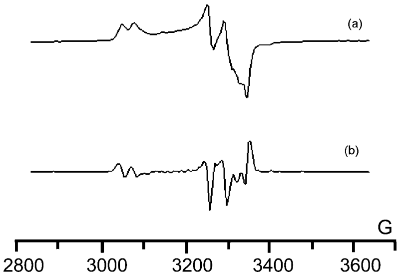

Figure 10. X-band EPR spectra of a THF solution of **2**: (a) first derivative spectrum; (b) second derivative spectrum. $T = 4.3$ K. Operational frequency $\nu = 9.39$ GHz.

Figure 12 shows the X-band EPR spectra of complex **5b** in THF solution.

The multiple derivative line shape analysis of the liquid-nitrogen spectrum has been carried out in terms of the $S = 1/2$ anisotropic Zeeman Hamiltonian. The intense signal is spectrally resolved in well-separated and narrow rhombic absorptions, with $g_{l,m,h}$ values significantly different from 2.0023 (see Table 6), which point out the metallic character of the SOMO.[24] No ^{61}Ni, ^{13}C, and ^{1}H couplings are detected.

At the glassy-fluid transition, the rhombic signals collapse in the corresponding narrow and unresolved isotropic absorption, the g_{iso} value of which well fits the $\langle g \rangle$ value. Rapidly refreezing the fluid solution totally recovers the previous glassy signals.

Figure 11. Second (a) and third (b) derivative X-band EPR spectra of $\mathbf{2}^{+}$ in THF solution at liquid-nitrogen temperature ($T = 100$ K). (c) Second derivative spectrum at $T = 298$ K. Operational frequency: $\nu = 9.69$ GHz. (Asterisks indicate noise spikes.)

As expected, the progressive anodic oxidation to $\mathbf{5b}^{+}$ affords a progressive decrease of the intensity of the signal recorded at 100 K.

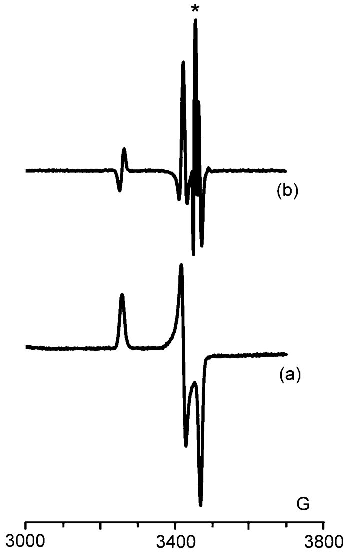

Figure 12. X-band EPR spectrum of **5b** in THF solution with first (a) and second (b) derivative modes at $T = 100$ K. Operational frequency: $\nu = 9.68$ GHz. (Asterisks indicate noise spikes.)

In the solid state, **5b** exhibits quite identical broad and unresolved rhombic line shapes and spectral parameters both at $T = 100$ and 298 K (see Table 6).

A similar paramagnetic behavior is displayed by **5a** both in the solution and solid states, with minor differences in line shapes and parameters.

It is noted that, as expected, the minor differences on the ligand frameworks of **5a**,**b** do not affect their magnetic features (a constant value of 1.83 μ_B has been calculated for both complexes either in the solid state or glassy solution, independently from the temperature).

Conclusions

The new nickelanickelocyclic **5a**,**b**, **5b**$^+$**PF**$_6$$^-$, and **4**$^+$**PF**$_6$$^-$ have been synthesized. In previous papers[5−7] we have shown that reactions of analogues of 1,4-dilithiobutadiene with nickelocene or pentamethylcyclopentadienylnickel acetylacetonate led to the formation of the five-membered nickelaindenyl and nickelafluorenyl cycles, showing that the nickelacycle can be bonded in η^5 or η^3 manner to the other metal atom when at least one of the double bonds of the "butadiene" fragment is part of the aromatic ring. Complexes **5a**,**b** and **5b**$^+$**PF**$_6$$^-$, in which the fortuitous addition of one hydrogen atom to butadiene destroys the aromaticity, are the first examples in which the five-membered nickelacycle can be bonded to the other nickel atom by η^4 bond type. Such bond type is similar to that reported by Brownstein[28] in the compound formed by the addition of the triphenylmethyl cation to one of the cyclopentadienyl rings in nickelocene.

We are still unsuccessful in preparing nickelocene analogues in which the central nickel atom would be bonded to the simple unsubstituted or substituted nickelacyclopentadienyl ring. Probably an additional stabilization of such ring is necessary.

On the basis of joint electrochemical and spectroelectrochemical studies, the apical Ni(II) site in complexes **2**−**4** formally undergoes the sequence Ni(IV)/Ni(III)/Ni(II)/Ni(I), thus mimicking the redox behavior of nickelocene, whereas the basal Ni(II) center only exhibits the Ni(II)/Ni(I) process. In complexes **5**, the apical Ni(II) center undergoes the sequence Ni(III)/Ni(II)/Ni(I), whereas the basal Ni(I) center exhibits the Ni(I)/Ni(II) process. In reality, the electron-transfer ability of the present complexes can be also theoretically described through fractional oxidation states.

Finally, the paramagnetic features of **2**/**2**$^+$ and **5a**,**b** have been determined by temperature-dependent X-band EPR spectroscopy.

Acknowledgment. P.Z. gratefully acknowledges the financial support of the University of Siena (PAR progetti 2005). P.B. and A.P. acknowledge the financial support of the Polish Ministry of Education and Science (Grant No. PBZ-KBN-118/T09/03).

IC701226D

---

(28) Brownstein, S. K.; Gabe, E. J.; Hynes, R. C. *Can. J. Chem.* **1992**, *70*, 1011.